Load Resistance of Masonry Infilled Panels for Steel Frames to Mitigate Progressive Collapse Caused by Middle Column Missing

Kai Qian[1*], Xi Lan[2], Xiao-Fang Deng[1], and Feng Fu[3]

[1] College of Civil Engineering, Guilin University of Technology, Guilin, China, 541004.

[2] College of Civil Engineering and Architecture, Guangxi University, Nanning, China, 530004.

[3] School of Mathematics, Computer Science and Engineering, City, University of London, U.K.

Abstract:

The load resistance of masonry infilled panels in upgrading the steel frame to mitigate progressive collapse was quantified experimentally and analytically in the current study. Four 1/2-scale steel subframes were tested, including two bare subframes without infilled panels for reference and two infilled subframes to assess the effects of infilled panels. Two types of connection were investigated in current study: welded connection and top and seat angle connection. The test result showed that infilled panels provided a greater improvement in initial stiffness and peak load of the steel subframe with top and seat angle connections compared to the infilled steel subframe with welded connections. On the premise that the connections retained their integrity, the strut mechanism of infilled panels could change from a diagonal strut mechanism forming in the whole panel to an off-diagonal strut mechanism formed in the remaining intact corner region with increasing vertical deflection. A novel equivalent multi-strut modelling method was proposed for the prediction of the infilled panel behavior with an acceptable level of accuracy. This model incorporates the shifts in the position of plastic hinges, which were influenced by the specific types of connection and the load-resisting mechanisms of the infilled panel. The analysis result demonstrated that the model slightly overestimated the load resistance of infilled panels within the steel frame with simple connections and slightly underestimated the load resistance of infilled panels within steel frame with semi-rigid or rigid connections.

Keywords: Progressive collapse; Steel frame; Infilled panel; Experimental; Connection type

* Corresponding author. E-mail address: qiankai@glut.edu.cn

1. Introduction

The consequence of the loss of one or a couple of structural members can be the collapse of the whole or substantial part of the building, which is the definition of progressive collapse. The most startling collapse was that of the World Trade Centre after the terrorist attack in 2001, in which the initial fracture triggered a cascade of failures of the structural members [1]. There are two common approaches to increase the load resistance against progressive collapse: (i) consider the potential vertical load resistance of non-structural members, such as masonry infilled panels (MIP); (ii) take advantage of the inherent contributions of secondary structural mechanisms, including compression arch action and catenary action.

Considering the potential load resistance of non-structural members is a more economical approach than strengthening buildings since the probability of progressive collapse events is low. It has been shown that MIP can mitigate vertical movement caused by column loss [2-4]. However, extra load resistance provided by MIP within reinforced concrete (RC) frames may require a compromise on structural ductility [5, 6]. Qian and Li [7] performed a pushdown experiment on an RC frame with solid MIP and reported that the load resistance of infilled RC frame reached its peak load at the beginning of test. Tsai and Huang [8] numerically investigated resistance of RC frames to progressive collapse, and nonlinear analysis indicated that the positive influence of brittle MIP disappeared once the infills began to fail. Compared to RC frames, steel frames tended to show a higher level of ductility and flexibility which may lead to different interactions between the MIP and the frames. However, there are few experimental studies focused on the influence of MIP in progressive collapse mitigation on the behavior of steel frame. Experimental results from Xavier et al. [9] indicated that steel frames could still maintain their load resistances even if the MIP were under severe damage in the large deflection stage, which is quite different to the RC frames. Brodsky et al. [10, 11] specialized in the study of tractive forces in the contact regions between frames and MIP. Although the overall response of infilled steel subframe was obtained through the above tests, load distribution via MIP and interactions between frame and MIP were still unclear.

The key to the latter approach is robust joints that provide considerable rotation capacity and catenary action capacity [12-14]. Yang and Tan [15] studied the steel subassemblies with typical bolted angle connections. They confirmed that flexural action was provided in the initial stage, while catenary action occurred when deflection exceeded one beam depth and gradually became the dominant load-resisting mechanism. Among the tested joints, the bolted angle connection performed most effectively in terms of catenary action development. Yu et al. [16] also evaluated the catenary action capacity of bolted angle connection, the test result indicated that the connections could provide considerable rotation capacity. Despite the popularity of bolted connections in Europe, a number of researchers have focused their attention on welded connections, which demonstrated reasonable performance and resistance to progressive collapse [17-20]. However, Li et al. [21] and Qian et al. [22] found that brittle fractures in welded connections decreased their rotation capacities, thus preventing catenary action development. Therefore, the connection types significantly influence the robustness of the steel frames.

Although some researchers have investigated the behavior of MIP in steel frames [23-25], the experimental studies on the effect of connection type on the resistance of infilled steel frame to progressive collapse are limited. Only Alrubaidi and Alhammadi [26] parametrically investigated the effectiveness of MIP on steel frame with different connections under progressive collapse. It is worth pointing out that due to the lack of infilled steel frame tests with different connections, the validation of their panel model was verified by the RC infilled frame tests [27]. Therefore, infilled steel frame tests with different connections need to be carried out to obtain experimental data as a basis for further analytical and finite element modelling studies.

For this purpose, four two-storey half-scale steel subframes with and without MIP were tested under a middle column removal scenario. The effects of MIP and connection types on the multi-storey steel subframes in mitigating progressive collapse were quantified. Moreover, the adaptability of the existing diagonal single-strut method was investigated and its ability to reproduce the progressive collapse responses of infilled steel frames with different connections was also qualified. As a result, novel multiple-strut models were proposed to simulate the progressive collapse responses of infilled panels under different load mechanisms. The applicability of the proposed multiple-strut models for

different connections was evaluated through a comparative analysis of the results from the tests and those of previous studies.

2. Experimental program

2.1. Specimen characteristics

To explore the behavior of infilled steel subframe under a middle column removal scenario, a six-storey steel frame building was designed as a prototype and two-span and two-storey specimens were fabricated as highlighted in Fig. 1. Ground column G4 was notionally removed before the test. Extending cantilever beams are fabricated beyond the extracted steel subframe for applying horizontal constraints to simulate that from neighbor bays.

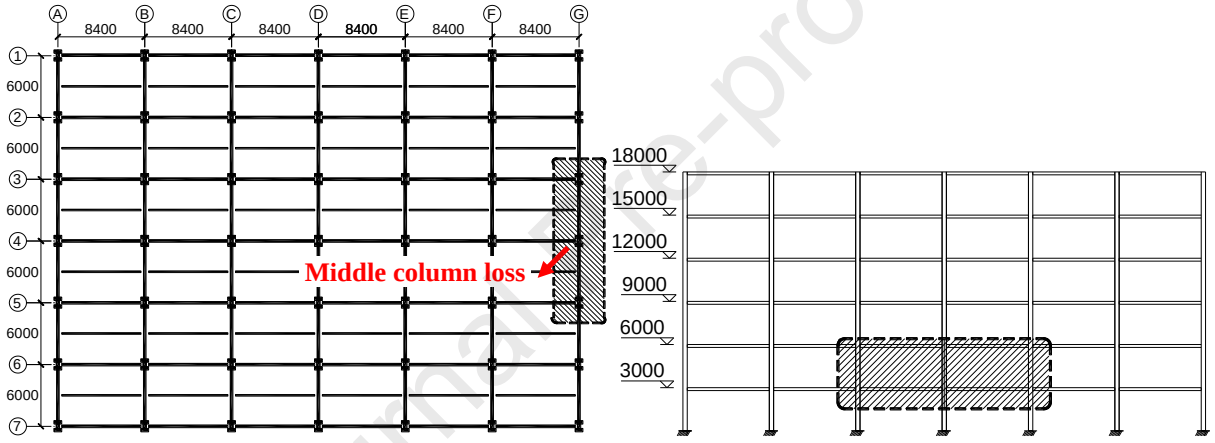

(a) (b)

Fig. 1 Position of extracted subframe (units: mm): (a) top view; (b) front view

In this study, four specimens were tested, including two bare subframes with welded connection or top and seat angle connection (WB and TSB), and two corresponding infilled subframes with welded connection or top and seat angle connection (WI and TSI). The infilled frames were designed following FEMA-356 [28], for which details are shown in Fig. 2. The half-scale specimens were tested, and the panel thickness was only 115 mm. The connection details, which were designed to meet ANSI/AISC-360-16 [29], are depicted in Fig. 3. With a frame span of 3.0 m, the floor height of the specimen is 1.5 m. The length of the beam extension beyond the side column was 0.655 m, which was used to provide lateral support from the neighboring bays. The column sections were HW 150×150×7×10 mm with continuous plates of 10 mm thickness installed in joints. The beam cross-section was HN

100 200×100×5.5×8 mm. For welded connections, full penetration welds were adopted to connect columns

101 and beams. For bolted connections, beams were fixed to the columns through steel angles with

102 dimensioned 70×8 mm and Grade 8.8 M18 bolts.

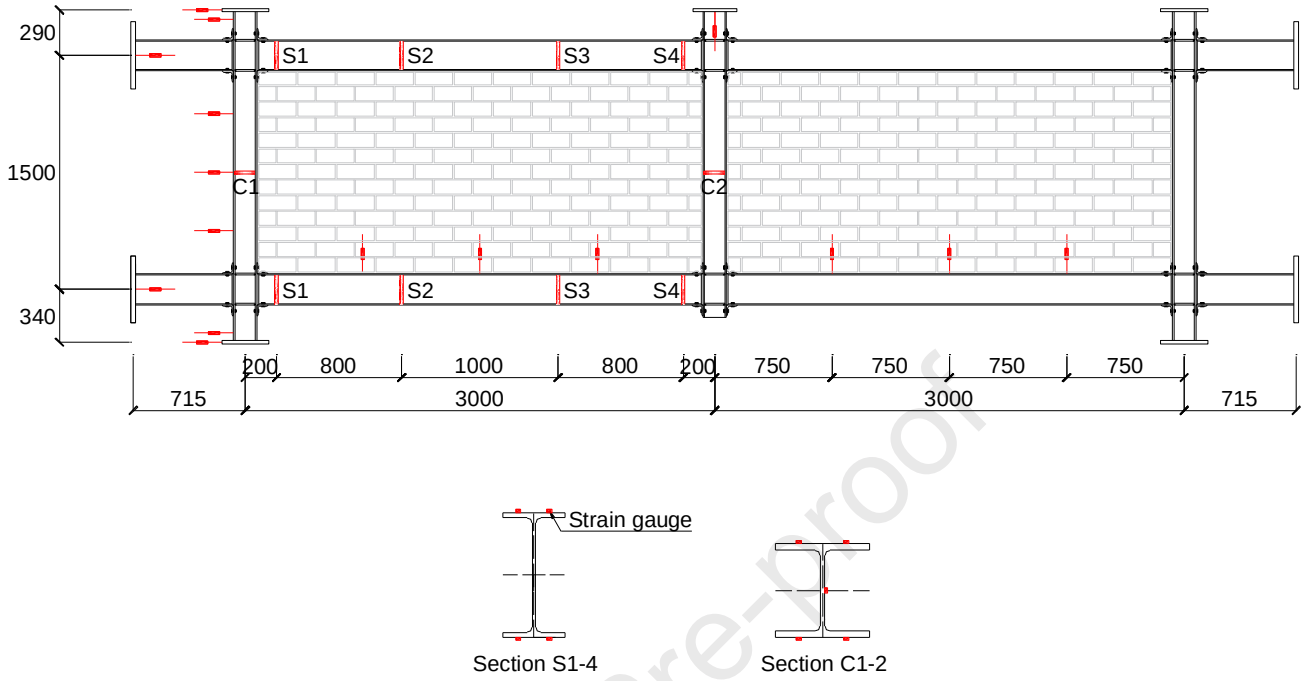

103

104 **Fig. 2** Layout of the infilled subframe and arrangement of the instrumentation system (units: mm).

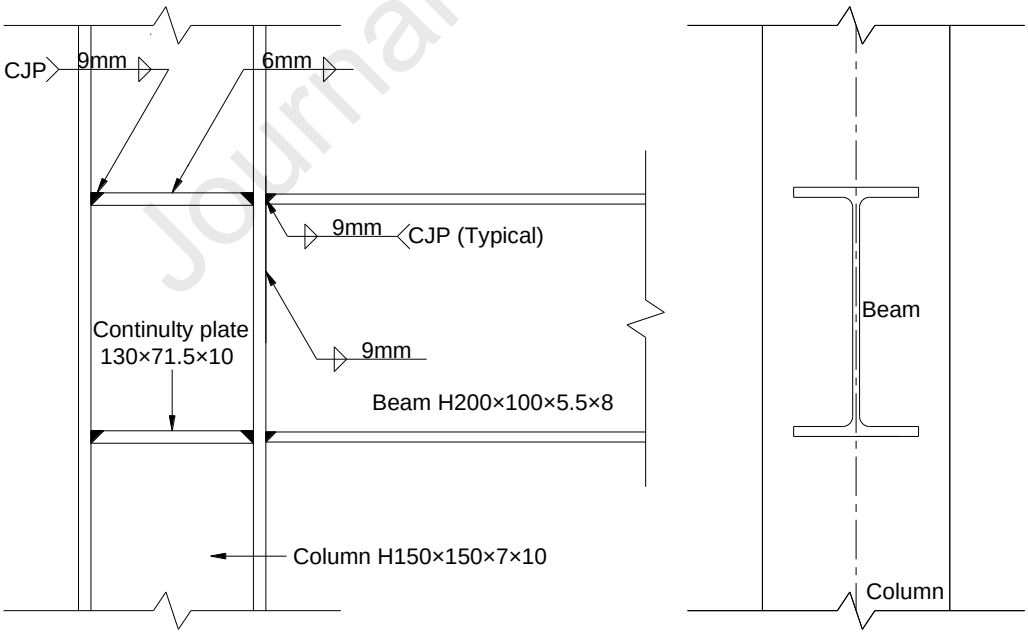

105

106 (a)

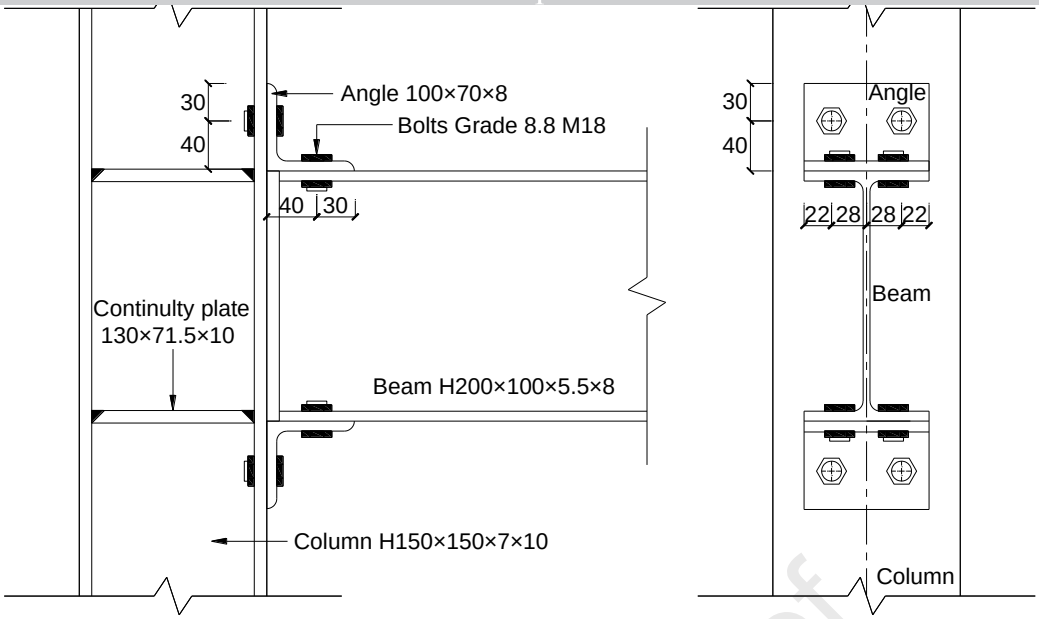

(b)

Fig. 3 Dimensional detail of connections (units: mm): (a) welded connection; (b) top and seat angle connection

2.2. Material properties

All MIPs were built from perforated bricks dimensioned 240×115×90 mm and a porosity of 35%. The compressive strength of brick and mortar was 9.8 MPa and 5.0 MPa, respectively. The compressive and shear strengths of the MIP (brick and mortar combination) were 3.7 MPa and 0.42 MPa, respectively. Material properties are tabulated in Table 1 for steel members.

Table 1: Materials

Items	Plate thickness (mm)	Yield strength (MPa)	Ultimate strength (MPa)	Yield strain	Ultimate strain	Elongation (%)
Beam flange	8.0	310	420	0.0019	0.0240	12.0
Beam web	5.5	320	430	0.0021	0.0249	13.5
Column flange	10.0	300	410	0.0019	0.0267	14.0
Column web	7.0	295	375	0.0023	0.0242	13.0
Angle	8.0	310	420	0.0019	0.0276	12.0

2.3. Test apparatus and instrumentations

Test apparatus and arrangements of instrumentations are presented in Figs. 2 and 4, respectively. A hydraulic jack is installed at the top of lost middle column to impose the concentrated loading using a deflection-controlled manner. A specially designed steel assemblage is fixed underneath the

hydraulic jack to eliminate out-of-plane movement. The bottom of side columns is mounted on the floor by pin supports. To simulate the axial load from the upper storeys, hydraulic jacks are installed at the top of side columns. The axial compression ratio is set to 0.3. Each of the extending cantilever beams beyond the side columns is linked to A-frame by chain poles.

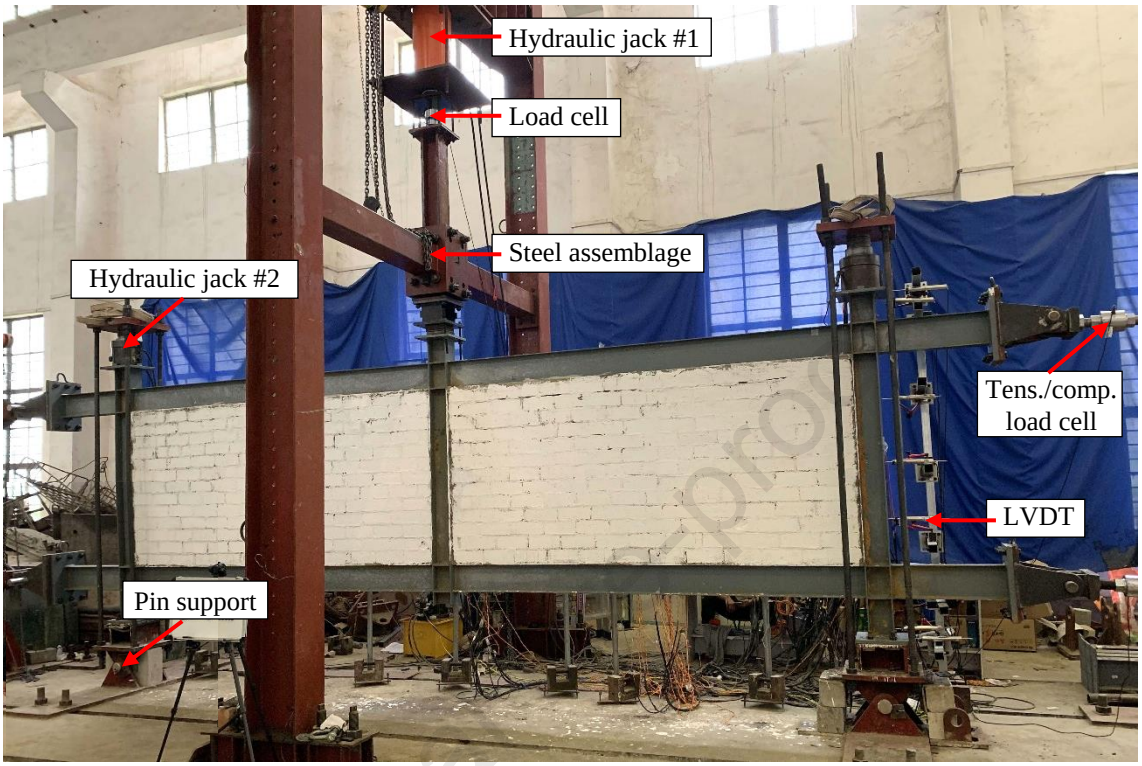

Fig. 4 Photograph of the test apparatus

The applied load on the middle column is monitored by a load cell beneath hydraulic jack. A load pin is mounted on each pin support to obtain its horizontal reaction. To monitor the horizontal reaction in chain pole, a tension/compression load cell is mounted at each chain pole. As given in Fig. 2, strain gauges are bonded to beams and columns to monitor the varying strain in critical sections. The internal force in subframes could therefore be determined using basic cross-sectional analysis. To monitor the deflection along beams and columns, deflection transducers are installed.

3. Experimental results

The aim of this paper is the quantification of the effect of MIP on the performance of steel subframes with different connections. Therefore, four steel subframes with or without MIP were tested and their principal characteristics are tabulated in Table 2.

Table 2. Experimental results

Specimen	U_{YL} (mm)	F_{YL} (kN)	K_{YL} (kN/mm)	U_{FPL} (mm)	F_{FPL} (kN)	U_{PL} (mm)	F_{PL} (kN)
WB	45	147.8	3.3	N/A	N/A	200	197.5
WI	21	217.1	10.6	49	246.9	352	248.8
TSB	20	13.5	0.7	N/A	N/A	394	44.4
TSI	10	54.2	5.4	80	109.1	334	119.9

Note: F_{YL}, F_{FPL}, and F_{PL} represent yield load, first peak load and peak load, respectively; U_{YL}, U_{FPL}, and U_{PL} represent deflections corresponding to the yield load, first peak load and peak load, respectively; K_{YL} denotes the counterpart initial stiffness to the yield load.

3.1. General behavior

Specimen WB

The load-deflection curve of WB is depicted in Fig. 5. A yield load of 147.8 kN was obtained at a middle column deflection (MCD) of 45 mm. Thus, initial stiffness, which is the ratio of yield load to corresponding deflection, was 3.3 kN/mm. Moreover, the peak load of 197.5 kN was obtained at the MCD of 200 mm. The weld fractures occurred in the lower beam (first storey beam) at this stage. With increasing vertical deflection, the fracture propagated into the beam web, leading to a slight reduction in load resistance. Although the load resistance increased again with the development of catenary action, the test eventually ended at 377 mm because of severe fractures in the middle joint of the upper beams. Failure mode of WB is illustrated in Fig. 6. Partial weld failure was noticed at Joint A, while complete weld fractures were recorded at Joints B and C.

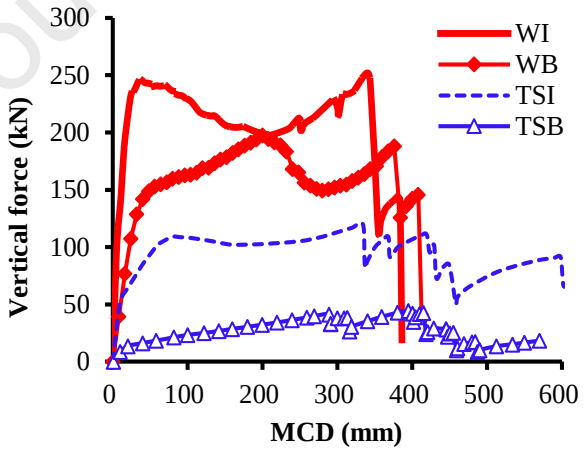

Fig. 5 Load-middle column deflection curves

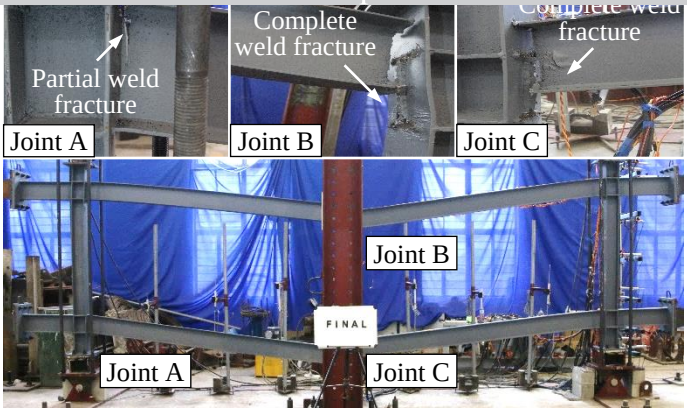

Fig. 6 Failure mode of WB

Specimen WI

Fig. 5 depicts the load-deflection curve of WI. Before reaching the MCD of 21 mm, diagonal and horizontal cracks (#1 in Fig. 7a) appeared in MIP and several cracks (#2 in Fig. 7a) also emerged in the top and bottom courses. The yield load and initial stiffness of WI were 217.1 kN and 10.6 kN/mm, respectively. First peak load of 246.9 kN was achieved at an MCD of 49 mm. With increasing deflection, the load resistance decreased as the diagonal cracks extended and increased in width. As a consequence, the load resistance re-ascended as a result of catenary action development in beams and load redistribution in MIP. After the slight drops in load resistance caused by the weld fractures in the side joints of lower beams at 251 mm and 351 mm, the peak load was achieved at 248.8 kN. The termination of test was because of the complete fracture of the side joints in upper and lower beams at MCDs of 352 mm and 383mm, respectively.

Figs. 7b and c illustrate the failure mode of WI. The MIPs were divided into three main parts: one diagonal region and two intact corner regions. As shown in Fig. 7b, the integrities of the MIP in corner regions were better than in diagonal regions. Moreover, the MIP detached with steel beams in the diagonal regions due to the beam torsion introduced by the infilled panel forces acting on the steel beams, for which the location could be ascertained by the buckling of the beam flanges. Regarding steel subframe, the joint fractures of WI are concentrated on the side joints in the lower beam because applied load was transmitted to the side columns through MIP.

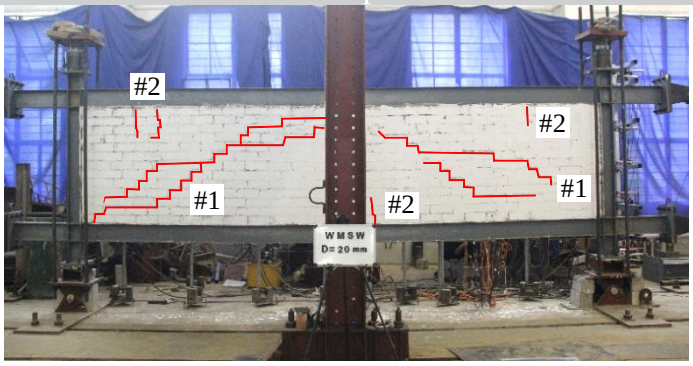

(a)

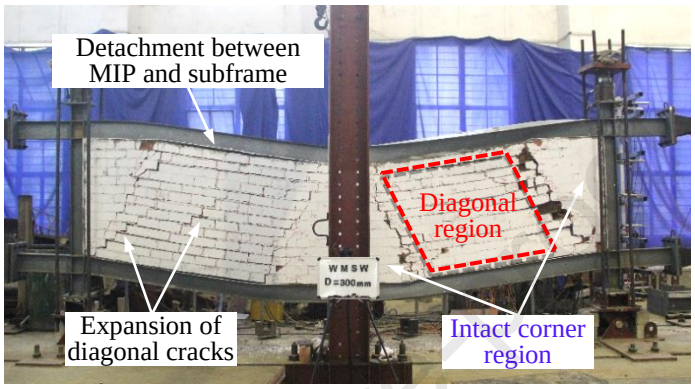

(b)

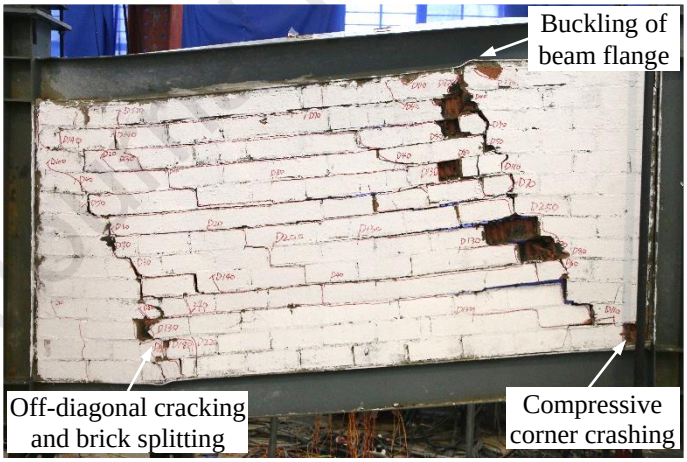

(c)

Fig. 7 Failure mode of WI: (a) MCD of 20 mm; (b) final cracking profiles; (c) detailed final damage of MIP

Specimen TSB

Fig. 5 illustrates load-deflection curve of TSB. Yield load of 13.5 kN was achieved at the MCD of 20 mm and initial stiffness was determined as 0.68 kN/mm. Tensile steel angles in lower beam successively fractured at MCDs of 291 mm and 316 mm. Although the failures were accompanied by

sudden drops, after a while, TSB continued to increase the load resistance and achieved a peak load of 44.4 kN at the MCD of 394 mm. This was because steel angles formerly under compression carried the tensile force after the failure of the tensile steel angles. The middle joints both failed before TSB reached its peak load. Thereafter, the tensile angles were fractured one after another, and the load resistance continued to decline. Failure mode of TSB is exposed in Fig. 8. Tensile steel angles in Joints A-E all fractured at test final.

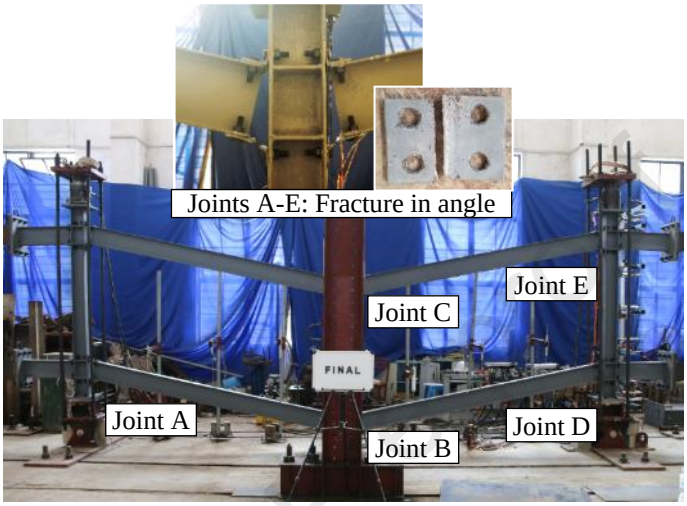

Fig. 8 Failure mode of TSB

Specimen TSI

Load-deflection curve of the TSI is displayed in Fig. 5. Horizontal and diagonal cracks (#1 in Fig. 9a) emerged in MIP at an MCD of 10 mm. Thereafter, although load resistance still increasing, the stiffness decreased significantly. Further increasing the deflection, several cracks developed in the corner of the MIP (#2 in Fig. 9a). TSI attained a first peak load of 109.1 kN at an MCD of 79 mm. As several diagonal cracks extended, the load resistance gradually declined. Subsequently, the load resistance rose again at an MCD of 170 mm until steel angle near middle column in lower beam fractured. Peak load of 119.9 kN was obtained at an MCD of 334 mm. As the sequential failures of tensile steel angles resulted in the limited catenary action capacity, load resistance during large deflection could not exceed the first peak load until test final.

Failure mode of TSI is displayed in Fig. 9b. A series of diagonal cracks formed in the MIP, with crushing and spalling at the compressive corner. The compressive angles in the connections underwent a large rotation deformation, while no contraction occurred in the MIP due to their high stiffness. This

resulted in the separation between MIP and steel joints in intact corner regions rather than in the diagonal region of WI. Failure mode of steel subframe was similar to that of TSB. All tensile steel angles but the one at side joint in upper beam were fractured.

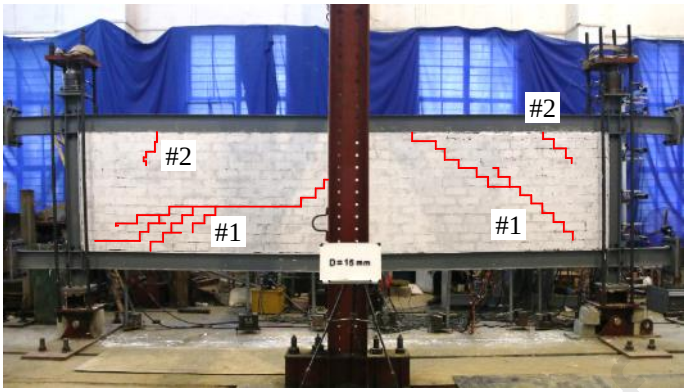

(a)

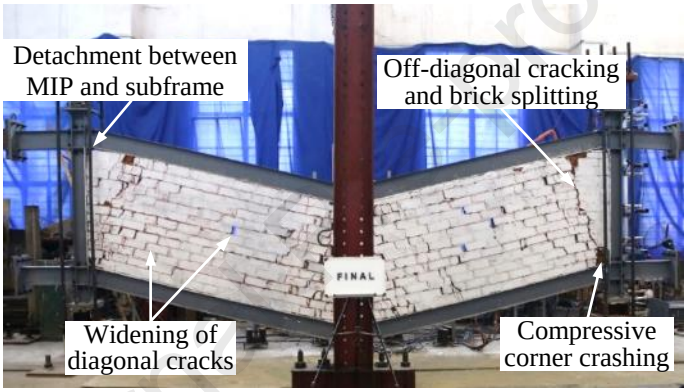

(b)

Fig. 9 Failure mode of TSI: (a) MCD of 15 mm; (b) final cracking profiles

3.2. Horizontal reactions

Fig. 10 is an illustration of the evolution of horizontal reactions, where positive and negative results denote tensile and compressive reactions, respectively. Maximum compressive forces of WB, WI, TSB, and TSI were -19.9 kN, -39.7 kN, -13.4 kN and -72.6 kN, respectively. Therefore, MIP significantly raised the maximum compressive forces of WB and TSB by 99% and 441%, respectively. As a consequence of the activation of catenary action, the maximum tensile forces of WB, WI, TSB, and TSI were 363.5 kN, 442.6 kN, 82.7 kN, and 82.0 kN, respectively. Therefore, the maximum tensile force of WI was 122% of that of WB because the existence of MIP prevented premature welding failure

at the steel subframe. However, for TSB and TSI, similar maximum tensile forces were measured because the steel angles started to fracture at a similar stage.

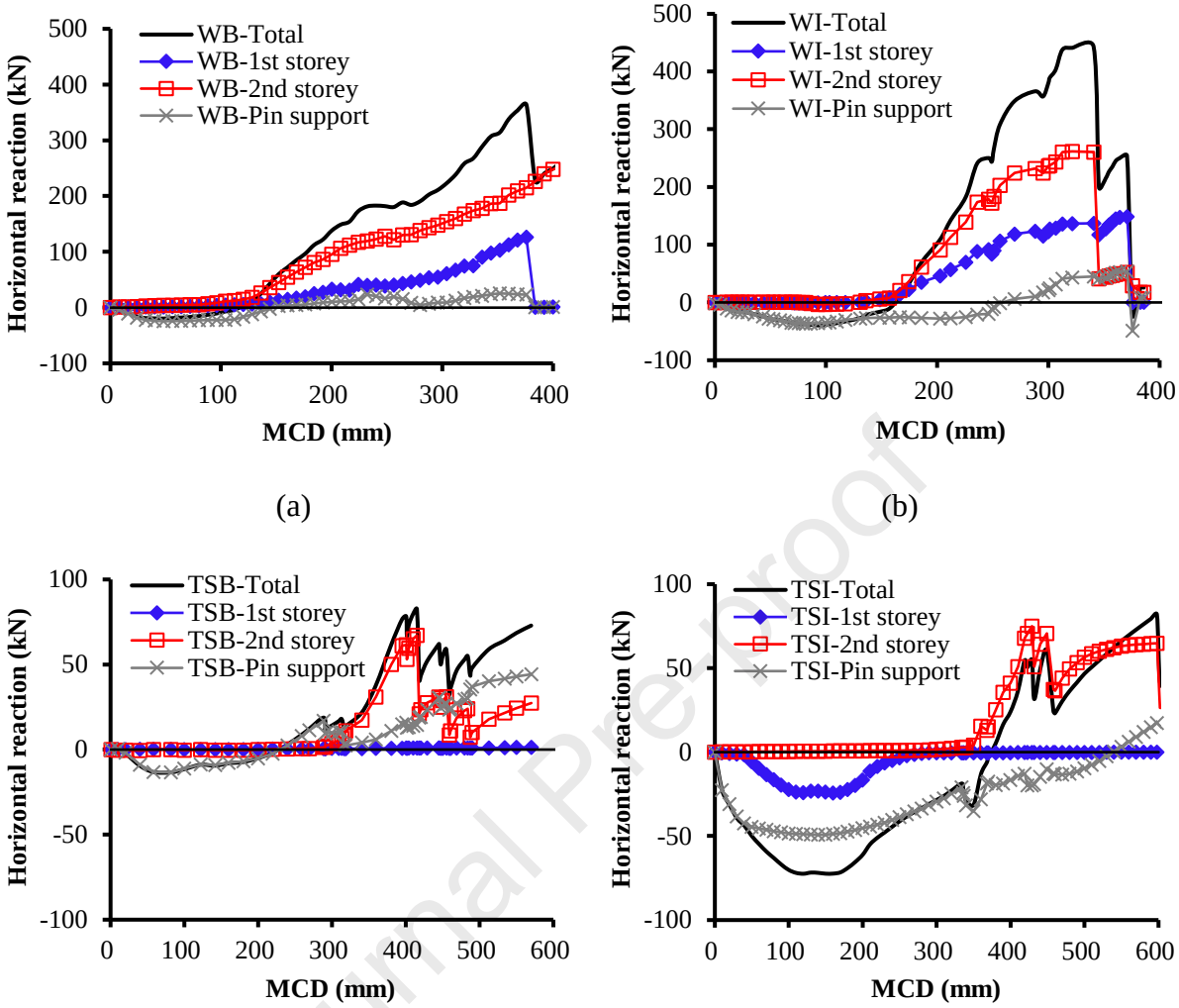

Fig. 10 Horizontal reaction-MCD curves: (a) WB; (b) WI; (c) TSB; (d) TSI

3.3. Deflection variation

The deflection shapes of the lower beams are shown in Fig. 11. The MIP would increase deflections of the lower beams. For WB and WI, the MIP changed the deflection shapes and the rotations of beam end close to the middle column were significantly overestimated by the chord rotation. This was due to the additional deflections induced by the MIP concentrated on the steel beams rather than the welding joints. For TSB and TSI, similar deflection shapes of beams were observed because the deflections were focused on the vulnerable steel angles rather than the beams. Similar observations were noted in prior investigations [30, 31].

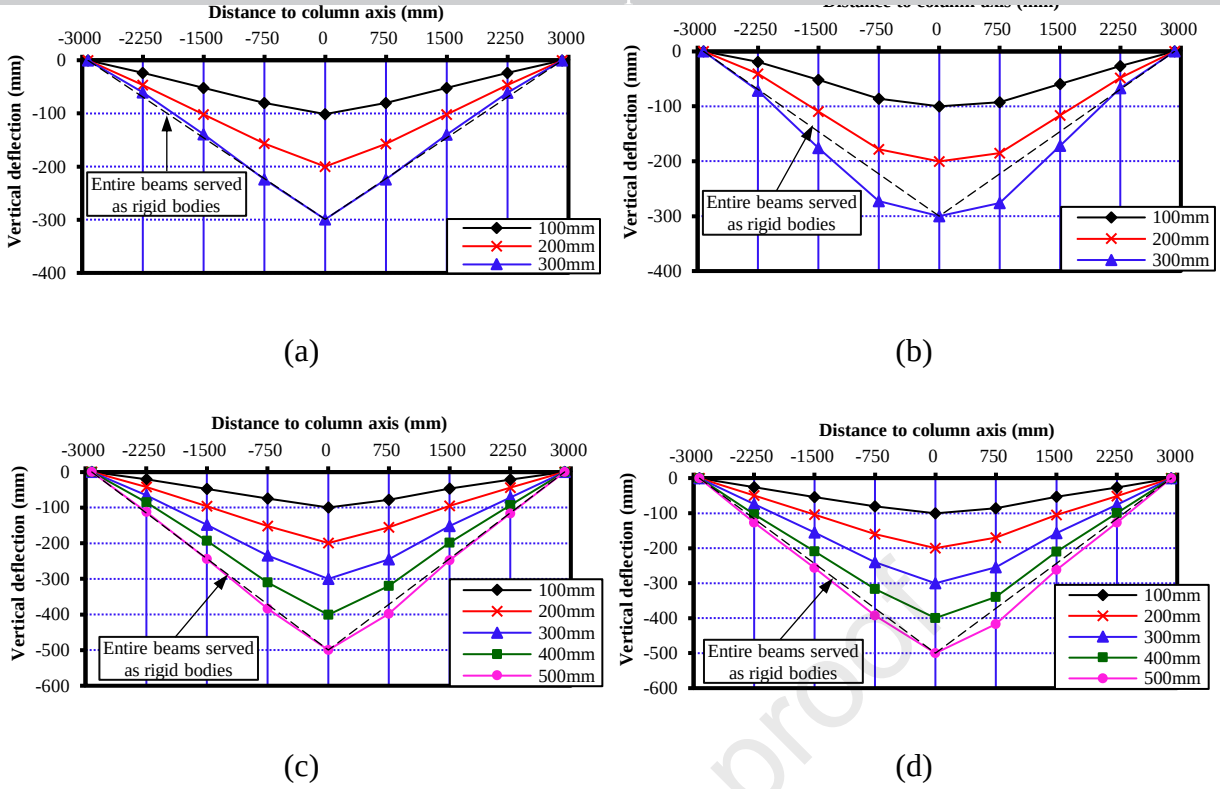

Fig. 11 Deflection shape of lower beams: (a) WB; (b) WI; (c) TSB; (d) TSI

4. Discussion of test results

4.1. Effects of MIP on steel subframes with different connection types

For the infilled subframes under middle column removal scenario, load redistribution was implemented via subframes and the interactions between MIP and subframes. As stiffness of MIP was significantly greater than that of steel beams, infilled subframes achieved much higher initial stiffness and peak load than that of corresponding bare subframes. As demonstrated in Fig. 5 and Table 2, MIP enhanced initial stiffness of WB and TSB by 221% and 694%, respectively. Peak loads of WI and TSI were 126% and 270% of the bare subframes, respectively. The test result indicated that MIP demonstrated a superior enhancement in initial stiffness and peak load capacity of infilled frame with top and seat angle connections in comparison to that with welded connections. This is because top and seat angle connections behave practically as a pin, with MIP serving the function of a diagonal strut. Consequently, the strut effectively transforms the quasi-unstable structure, comprising columns and beams connected by four pins, into a stable and stiff truss structure. In contrast, the welded connection

provides the frame with stability and stiffness. Therefore, in the case of welded connections, the contribution of diagonal strut is significantly diminished.

Table 2 presents the deflection capacities, which were determined as vertical deflection at peak load, of WB, WI, TSB, and TSI were 200 mm, 352 mm, 394 mm, and 334 mm, respectively. The deflection capacity of WI and TSI was therefore 176% and 85% of that of the bare subframe, respectively. This was because the presence of the remaining MIP in WI transferred the positions of the plastic hinges from joints to steel beams, which prevented the premature fracture of joints. However, the additional shear forces generated by the MIP concentrated on the relatively weak joints, resulting in a reduction of the deflection capacity of TSI. Therefore, in addition to panel failures, the steel frame may also experience beam, column or connection failures as a consequence of the concentrated forces that the struts apply on the steel structure during the process of resisting progressive collapse. The potential for the MIP to play a role in load redistribution is contingent upon the steel frame retaining its structural integrity, as the efficacy of this redistribution is dependent on the interaction between the MIP and the frame. In cases where MIPs are designed to resist progressive collapse, it is of paramount importance to conduct further checks on the steel frame, in order to prevent the potential premature failure resulting from the steel frame forces generated by the MIP.

Fig. 12 decomposes load resistance from flexural action and catenary action based on the internal force measurements of strain gauges installed in key sections of beams. The detailed calculation method of calculation has been described in a previous paper by the authors. [32]. For the subframes with welded connections and top and seat angle connections, the load resistance was entirely due to flexural action before MCD reached 170 mm and 300 mm, respectively. The flexural action in WI was greater than WB before reaching its peak load, but eventually, WI reached a similar level of flexural action as WB. The MIP increased the maximum contribution of flexural action in TSI by 42% compared to TSB. Catenary action of WB, WI, TSB, and TSI was motivated at vertical deflections of 128 mm, 167 mm, 241 mm, and 290 mm, respectively. Therefore, the MIP would delay the activation of catenary action by 20-30% of the vertical deflection.

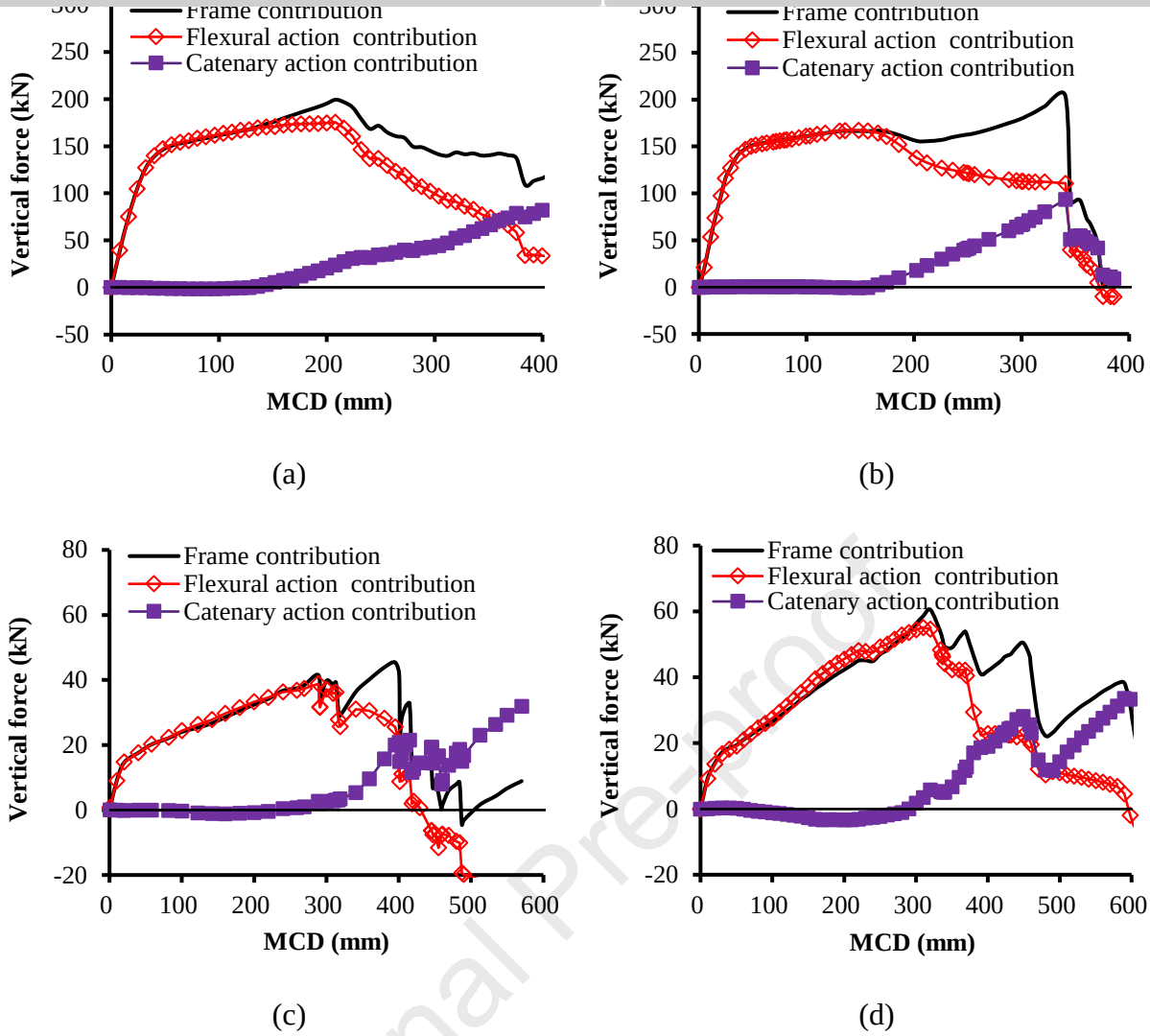

Fig. 12 De-composition of frame contribution: (a) WB; (b) WI; (c) TSB; (d) TSI

4.2. Load distribution mechanism of MIP at different stages

Figs. 13a and b illustrate the two strut mechanisms of MIP observed in the test, diagonal strut mechanism and off-diagonal strut mechanism. These mechanisms have also been observed in previous research [33-35]. With the increasing deflection, the strut mechanism changes from diagonal strut mechanism forming in the whole panels (Fig. 13a) to off-diagonal strut mechanism forming in the remaining intact corner region (Fig. 13b). As evidenced by the failure modes in Figs.7b and 9b, the intact corner regions in WI were much larger than those in TSI because of the different plastic hinge positions formed by MIP on the steel beams, which will be further explained in Section 5.1.

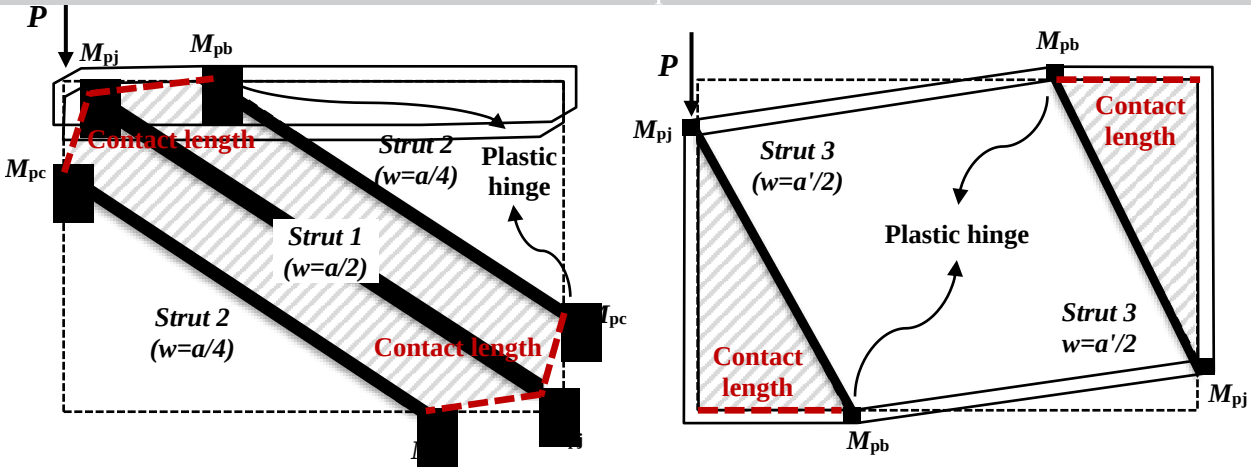

(a) (b)

Fig. 13 Strut mechanism of MIP within the steel subframe: (a) diagonal strut mechanism; (b) off-diagonal strut mechanism

As presented in Fig. 14, load contribution from MIP in the infilled subframes is quantified through the subtraction of the load resistance of steel subframe (frame contribution in Fig. 12) from the total resistance of infilled subframes. For a simplified design, the behavior of MIP within a steel frame is assumed to act as struts. At the initial stage, the enhancement of load resistance was provided by the diagonal struts in MIP (see Fig. 13a). These diagonal struts were effective until the diagonal cracks visibly widened. The diagonal strut resistances of MIP in WI and TSI were 119.2 kN and 85.2 kN, respectively. Thus, the diagonal strut resistance of MIP in WI was 40% greater than that of TSI. However, the formation of struts in MIP was accompanied by an increasing shear force imposed on the beam-column connections. This may cause the connections to fail prematurely and the load resistance of infilled subframes to reach their maximum resistance before the mobilization of catenary action. If the connections survived during the large deflection behavior of beams, the load resistance of the infilled subframes increased again due to the off-diagonal struts (see Fig. 13b) formed in the remaining MIP and catenary action developed in the steel subframe. The load resistances of off-diagonal struts were eventually stabilised at a certain level, where those in WI and TSI were 43.7 kN and 56.6 kN respectively.

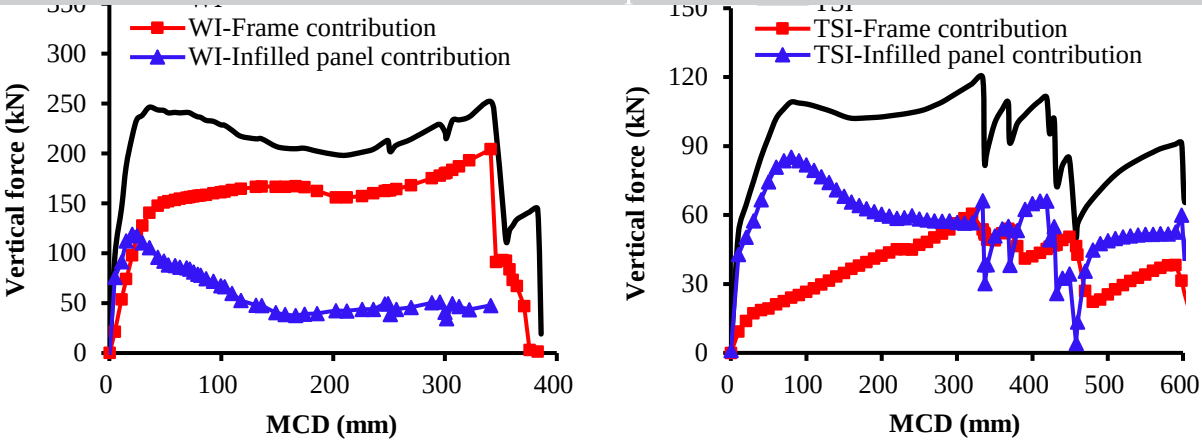

(a) (b)

Fig. 14 De-composition of load resistance from infilled steel frame: (a) WI; (b) TSI

5. Adaptation of equivalent strut model for the reproduction of the progressive collapse behavior of infilled steel frame

In previous studies [7, 36, 37], equivalent strut methods have been tested and demonstrated satisfactory approximation of the experimental results. These authors eventually proposed a fixed geometry diagonal single-strut method, which was deemed appropriate for the aforementioned case but was found to be inconsistent with the findings in the current test. The test result demonstrated that the strut mechanisms exhibited variation with the increase in middle column deflection. Concurrently, the position of the strut acting on the steel frame (i.e., the contact length between MIP and frame) varied with the connection type under identical strut mechanisms.

This section presents an investigation into the applicability of the proposed multiple-strut model in simulating the progressive collapse behavior of the infilled frame. For the two strut mechanisms of MIP outlined in Section 4.1, two potential configurations of models in use for the assessment of the MIP resistance at varying stages: the diagonal strut configuration at the first peak load stage (see Fig. 13a) and the off-diagonal strut configuration at the peak load stage (see Fig. 13b). For diagonal strut configuration illustrated in Fig. 13a, the struts 2 are situated at the end of contact length, which depends on the specific connection type of the infilled frame. The methodology for defining the contact length is presented in Appendix A. In the off-diagonal strut configuration, as illustrated in Fig. 13b, the two off-diagonal struts originate at the end of the failed diagonal strut and extend towards the upper and

lower beams at a distance equal to the contact length, which is also dependent on the connection type of the infilled frame. The struts 3 are employed in the modelling of the observed failure mechanism of MIP, whereby the panel at the corners remains intact, while the panel in the diagonal area is cracked.

These evaluations are performed for the currently tested specimens with welded connections and top and seat angle connections. To extend the comparison of different connections in the accuracy of prediction, the results of previous finite element studies [9, 26, 37] are also evaluated. Details of the strut definitions are provided in Appendix B. Table 3 shows the results of the comparison, which demonstrates an acceptable degree of accuracy.

Figs. 15a and b illustrate the effect of the strength ratio of bare frame to infilled frame (ζ) on the accuracy of proposed model for different connections. As demonstrated by the data presented in Table 3, the collected data can be classified into two categories: frames with simple connections ($\zeta < 0.05$) and frames with semi-rigid or rigid connections ($\zeta \geq 0.05$). As shown in Fig. 15a, at the peak load stage, diagonal strut configuration model overestimates the resistance of the MIP within the steel frame with simple connections within 23% and underestimates that with semi-rigid and rigid connections within -29%. This is justified because the diagonal strut configuration model was originally validated only by the infilled frame comprising semi-rigid connections and elastic frame elements. As illustrated in Fig. 15b, for the MIP resistance during the peak load stage, the models with off-diagonal strut configurations exhibit a tendency to produce underestimated predictions for MIP in steel frame with semi-rigid or rigid connections within -16%, with the exception of the infilled frame with the welded connections (WI). The overestimation of the predictions in WI is due to the plastic bending moments of the frames being determined by the steel beams rather than the connections in bare frames. Nevertheless, both the diagonal strut configuration model and the off-diagonal strut configuration proposed in this paper are considered to be simple and effective solutions for estimating the resistance of infilled frame undergoing progressive collapse during first peak load stage and peak load stage, respectively.

359 **Table 3:** Summary of key test results and analytical results of strut model

Authors	Connection type	Measured resistance of bare frame (kN)		Measured resistance of infilled frame (kN)		Measured resistance of MIP (kN)		Analytical resistance of MIP (kN)		Analytical/Measured result of MIP resistance	
		First peak load	Peak load	First peak load	Peak load	First peak load	Peak load	Diagonal strut model for first peak load stage	Off-diagonal strut model for peak load stage	First peak load	Peak load
Xavier et al. [10]	Web cleat connection	14	N/A	345	N/A	331	N/A	407	N/A	1.23	N/A
Shan et al. [37]	Rigid connection	270	543	1265	1315	995	772	771	711	0.77	0.92
Alrubaidi and Alhammadi [26]	Fin-plate connection	9	N/A	891	N/A	882	N/A	1051	N/A	1.19	N/A
	Extended end-plate connection	1022	N/A	2227	N/A	1205	N/A	1020	N/A	0.85	N/A
	Welded connection	1893	N/A	3334	N/A	1441	N/A	1027	N/A	0.71	N/A
This test	Welded connection	148	198	247	249	99	51	76	63	0.77	1.24
	Top and seat angle connection	14	44	109	120	95	76	74	64	0.78	0.84

360

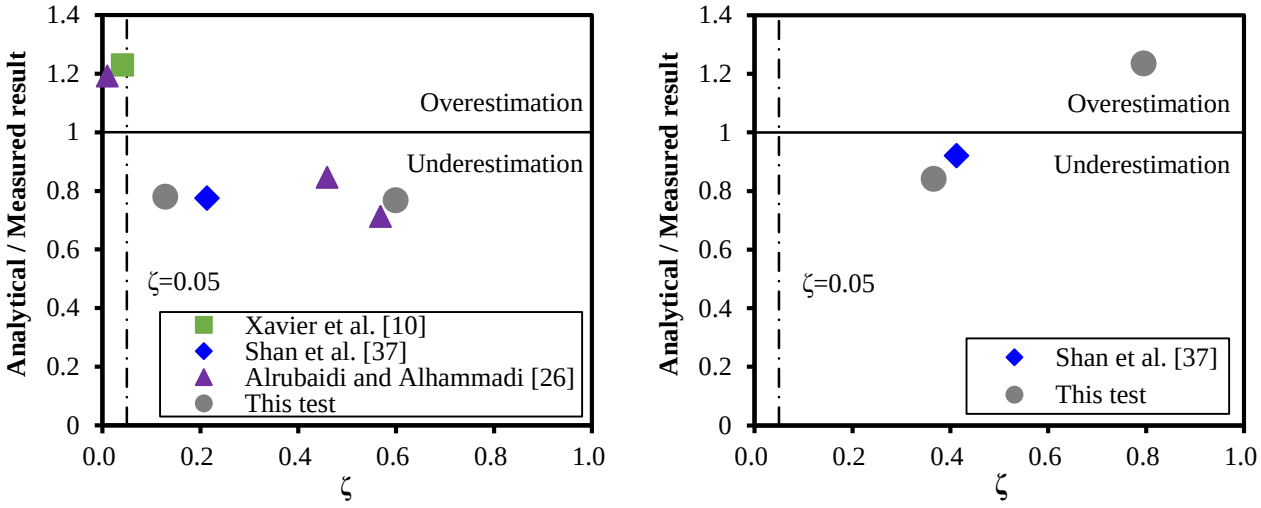

Fig. 15 Effect of the strength ratio of bare frame to infilled frame (ζ) on the accuracy of proposed model: (a) diagonal strut configuration (b) off-diagonal strut configuration

6. Conclusions

Conclusions can be obtained from the results of the experiments as follows:

1. Due to the significant masonry stiffness, the initial stiffness of WB and TSB was 321% and 794% of that of the bare subframes, respectively. Moreover, the infilled panels allowed a vertical load imposed on a middle column to be distributed to the side columns and steel beams. Thus, the infilled panels increased the peak load of WB and TSB by 26% and 170%, respectively. Test results suggested that the infilled panels provided a greater improvement in initial stiffness and peak load of infilled steel subframe with top and seat angle connections compared to that of infilled steel subframe with welded connections. This was because the infilled panels transformed the steel frame with top and seat angle connections, from an unstable structure to a stable and rigid truss structure while the steel frame with welded connections demonstrated inherent stability and rigidity. The deflection capacity of WI was 176% of that of WB due to the infilled panels changing the position of plastic hinges in steel beams, while the additional shear forces generated by the infilled panels reduced the deflection capacity of TSI by 15%.

2. For the bare subframes, the main load-resisting mechanism was flexural action initially. During the large deflection stage, flexural action was combined with catenary action to resist the applied load.

For infilled subframes, load-resisting mechanisms of the steel subframes were similar to those of the bare subframes. However, the sequential mobilization of the diagonal and off-diagonal strut mechanisms in the infilled panels delayed the initiation of catenary action.

3. Failure modes identified in tests indicated that, during the initial stage, the infilled panels within steel frame transferred the applied load via diagonal struts. With increasing deflection, the strut mechanism of the infilled panels changed from diagonal strut mechanism forming in the whole panel to off-diagonal strut formed in the remaining intact corner region. The resistance decomposition of steel subframes and panels in infilled subframes showed that the infilled panels were still able to provide considerable load resistance during the off-diagonal strut mechanism stage.

4. The proposed multi-strut model is adapted in a simple way to capture the progressive collapse response of infilled panels by incorporating the effect of different connections in the surrounding steel frames and different load mechanisms in the infilled panels. The analysis result illustrates that the method slightly overestimates the panel resistance within the steel frame with simple connections and slightly underestimates the load resistance of infilled panels within steel frame with semi-rigid or rigid connections.

Acknowledgements

This research was supported by a research grant provided by the National Natural Science Foundation of China (Nos.52022024, 52168028) and Natural Science Foundation of Guangxi (No.2021GXNSFFA196001). Any opinions, findings and conclusions expressed in this paper are those of the writers and do not necessarily reflect the view of National Natural Science Foundation of China.

Data availability

Some or all data, models, or code that support the findings of this study are available from the corresponding author upon reasonable request.

Appendix A. Contact length of MIP within steel frames with different connections

The contact lengths between MIP and steel subframe are shown in Fig.14. Different from the unconfined panels, once the diagonal cracks develop in the panels, they find themselves constrained by the surrounding frames and resist them via contact lengths. Considering the static moment of the

force acting on beams and columns, Sahelnejad and Hobbs [35] proposed that the contact lengths on beams and columns are given in Eqs. (1)-(2). According to Eq. (1), due to the greater moment resistance provided by welded connections, longer contact lengths are generated in the infilled frames with welded connections compared to that with top and seat angle connections, which are consistent with failure modes during tests (see Figs.7b and 9b).

$$\alpha_b l_b = \sqrt{\frac{2\left(M_{pj} + 0.2M_{pb}\right)}{f_m t_{\inf}}} \le 0.4 l_b \tag{1}$$

$$\alpha_c h_{col} = \sqrt{\frac{2\left(M_{pj} + 0.2M_{pc}\right)}{f_{m-0} t_{\inf}}} \le 0.4 h_{col} \tag{2}$$

where α_b and α_c represent the ratio of contact length over beam span (l_b) or column height (h_{col}), respectively; M_{pj} represents the plastic moment of joint, which is the minimum of the plastic moment capacity of beam, column and connection, which will be presented below; M_{pb} and M_{pc} represents plastic moment of beam and column, respectively; f_m and f_{m-0} are compressive strength of masonry parallel and normal to bed joint, respectively; $t_{\inf}$ is thickness of MIP.

For infilled steel frame with welded connection, the plastic moment capacity is generally controlled by the beams or columns, while the one in the infilled steel frame with top and seat angle connections is controlled by connections and evaluation method has been provided by Qian et al. [38], especially for the plastic moment of top and seat angle connections:

$$M_{p,ts} = \frac{\beta f_{y,a} h_b b_a t_a^{\,2}}{4 g_a} \tag{3}$$

where β represents the coefficient for precisely estimating the influence of variables that influence the failure pattern, as proposed by Pirmoz et al. [39]; $f_{y,a}$ represents angle yield strength; h_b represents beam depth; b_a and t_a are width and thickness of angle, respectively; g_a is gage distance between back of angle and axis of bolts on beam.

Appendix B. MIP resistance for different strut mechanisms

As shown in Fig.14, the application of a multi-strut model allows the interaction between MIP and the steel frame to be taken into account, since load transfers from frame elements to MIP depend on contact lengths (the struts are located at the ends of contact length), instead of using a single diagonal strut (Strut 1). Therefore, two additional off-diagonal struts (Struts 2) are suggested in this paper, which is widely adopted in previous research [40, 41]. Considering the diagonally loaded panel consists of two diagonal regions, the panel is assumed to be the struts with a total width of a and each region of the panel is half the strut width $a/2$. Furthermore, each region is replaced by two struts, each of width $(a/2)/2 = a/4$. Among them, the two struts in the diagonal direction are merged into diagonal strut width of $2(a/4) = a/2$, as shown in Fig.14a.

The off-diagonal strut mechanism shown in Fig.14b appeared after the failure caused by extensive diagonal cracks. The acting positions of the two new off-diagonal struts (Struts 3) can be identified by the plastic hinges formed on steel beams. Instead of the panel length used in diagonal strut mechanism, the effective width of the intact corner region is taken to be the beam contact length. The beam contact length in the off-diagonal strut mechanism is limited to $0.35l_b$ [42], which is different from the diagonal strut mechanism. Similar to diagonal strut model, off-diagonal strut width is determined as $a'/2$.

Based on the above assumptions relating to strut formation, the load resistance of MIP for different strut mechanisms can be determined. The contact lengths between MIP and steel subframe with different connections that are calculated in Eqs. (1)-(3) are then substituted into Eqs. (4)-(6), which are provided by FEMA-356 [28], to predict the load resistance prediction of MIP.

$$R_{inf} = at_{inf} f_m \sin\theta \tag{4}$$

$$a = 0.175\left(\lambda h_{inf}\right)^{-0.4} r_{inf} \tag{5}$$

$$\lambda = \left[\frac{E_m t_{inf} \sin 2\theta}{4E_s I_{col} h_{inf}}\right]^{\frac{1}{4}} \tag{6}$$

where R_{inf} is the load resistance of MIP; d is strut width; λ is a parameter to determine strut width; θ is the angle between the strut and steel beam; I_{col} is the column inertia moment; r_{inf} and h_{inf} represent diagonal length and height of infilled panel, respectively; E_m and E_s are elasticity modulus of masonry and steel frame, respectively.

References

[1] NIST, Federal building and fire safety investigation of the world trade center disaster: Structural response and probable collapse sequence of world trade center building 7, National Institute of Standards and Technology Report NIST NCSTAR 1-9, 2008.

[2] Shan, S., Li, S., Xu, S., Xie, L., Experimental study on the progressive collapse performance of RC frames with infill walls, Eng. Struct. 111 (2016) 80-92.

[3] Sasani, M., Response of a reinforced concrete infilled-frame structure to removal of two adjacent columns, Eng. Struct. 30(9) (2008) 2478-2491.

[4] Wang, F., Yang, J., Wang, X.-e., Azim, I., Study on progressive collapse behaviour of steel-framed substructures with sheathed CFS stud infill walls, J. Build. Eng. 42 (2021) 102720.

[5] Brodsky, A., Yankelevsky, D.Z., Resistance of reinforced concrete frames with masonry infill walls to in-plane gravity loading due to loss of a supporting column, Eng. Struct. 140 (2017) 134-150.

[6] Buitrago, M., Bertolesi, E., Sagaseta, J., Calderon, P.A., Adam, J.M., Robustness of RC building structures with infill masonry walls: Tests on a purpose-built structure, Eng. Struct. 226 (2021) 111384.

[7] Qian, K., Li, B., Effects of masonry infill wall on the performance of RC frames to resist progressive collapse, J. Struct. Eng. 143(9) (2017) 04017118.

[8] Tsai, M.H., Huang, T.C., Numerical investigation on the progressive collapse resistance of an RC building with brick infills under column loss, Int J Civil Environ Struct Constr Archit Eng 5(10) (2011) 483-490.

[9] Xavier, P.B., Macorini, L., Izzuddin, B.A., Chisari, C., Gattesco, N., Noe, S., Amadio, C., Pushdown tests on masonry infilled frames for assessment of building robustness, J. Struct. Eng. 143(9) (2017) 04017088.

[10] Brodsky, A., Rabinovitch, O., Yankelevsky, D.Z., Determination of the interaction between a masonry wall and a confining frame, Eng. Struct. 167 (2018) 214-226.

[11] Brodsky, A., Rabinovitch, O., Yankelevsky, D.Z., Effect of masonry joints on the behavior of infilled frames, Constr. Build. Mater. 189 (2018) 144-156.

[12] Qian, K., Weng, Y.-H., Zhang, L., Li, Z., Lan, X., Feasibility of two-storey substructures to equivalently investigate behaviour of multi-storey steel frames, J. Constr. Steel Res. 210 (2023) 108088.

[13] Lan, X., Li, Z., Fu, F., Qian, K., Robustness of steel braced frame to resist disproportionate collapse caused by corner column removal, J. Build. Eng. 69 (2023) 106226.

[14] Lan, X., Wang, Y., Tan, B., Zhang, Y., An assessment of application of the component-based method to full range behaviour of joints between steel beam to concrete filled steel tube columns under extreme loading conditions, Eng. Struct. 309 (2024) 118057.

[15] Yang, B., Tan, K.H., Experimental tests of different types of bolted steel beam-column joints under a central-column-removal scenario, Eng. Struct. 54 (2013) 112-130.

[16] Yu, H., Burgess, I.W., Davison, J.B., Plank, R.J., Tying capacity of web cleat connections in fire, part 2: Development of component-based model, Eng. Struct. 31(3) (2009) 697-708.

[17] Li, L., Wang, W., Chen, Y., Teh, L.H., Column-wall failure mode of steel moment connection with inner diaphragm and catenary mechanism, Eng. Struct. 131 (2017) 553-563.

[18] Lew, H.S., Main, J.A., Robert, S.D., Sadek, F., Chiarito, V.P., Performance of steel moment connections under a column removal scenario. I: Experiments, J. Struct. Eng. 139(1) (2013) 98-107.

[19] Sadek, F., Main, J.A., Lew, H.S., Bao, Y.H., Testing and analysis of steel and concrete beam-column assemblies under a column removal scenario, J. Struct. Eng. 137(9) (2011) 881-892.

[20] Li, H.H., Cai, X.H., Zhang, L., Zhang, B.Y., Wang, W., Progressive collapse of steel moment-resisting frame subjected to loss of interior column: Experimental tests, Eng. Struct. 150 (2017) 203-220.

[21] Li, L.-L., Li, G.-Q., Jiang, B., Lu, Y., Analysis of robustness of steel frames against progressive collapse, J. Constr. Steel Res. 143 (2018) 264-278.

[22] Qian, K., Lan, X., Li, Z., Fu, F., Effects of steel braces on robustness of steel frames against progressive collapse, J. Struct. Eng. 147(11) (2021) 04021180.

[23] Qu, Z.-Y., Zhong, W.-H., Tan, Z., Chen, J.-L., Wang, H.-C., Research on the anti-collapse performance of steel frame structures with infilled walls in the form of reduced beam sections connections, J. Build. Eng. 91 (2024) 109600.

[24] Zhang, J.-Z., Chen, X., Li, G.-Q., Yu, Z.-W., Collapse mechanism of three-dimensional modular steel buildings: Effect of steel wall and difference with traditional steel frame, J. Build. Eng. 76 (2023) 107197.

[25] Wang, J.-X., Sun, Y.-H., Gao, S., Wang, W.-D., Anti-collapse mechanism and reinforcement methods of composite frame with CFST columns and infill walls, J. Constr. Steel Res. 208 (2023) 108022.

[26] Alrubaidi, M., Alhammadi, S.A., Effectiveness of masonry infill walls on steel frames with different beam-column connections under progressive collapse, Structures 38 (2022) 202-224.

[27] Li, S., Shan, S., Zhai, C., Xie, L., Experimental and numerical study on progressive collapse process of RC frames with full-height infill walls, Eng. Fail. Anal. 59 (2016) 57-68.

[28] FEMA356, Prestandard and commentary for the seismic rehabilitation of buildings, Washington, D.C: Federal Emergency Management Agency, 2000.

[29] ANSI/AISC-360-16, Specification for structural steel buildings, Chicago, Illinois, USA: American Institute of Steel Construction, 2016.

[30] Hasan, M.J., Ashraf, M., Uy, B., Moment-rotation behaviour of top-seat angle bolted connections produced from austenitic stainless steel, J. Constr. Steel Res. 136 (2017) 149-161.

[31] Kong, Z., Kim, S.-E., Numerical estimation for initial stiffness and ultimate moment of top-seat angle connections without web angle, J. Struct. Eng. 143(10) (2017) 04017138.

[32] Qian, K., Lan, X., Li, Z., Li, Y., Fu, F., Progressive collapse resistance of two-storey seismic configured steel sub-frames using welded connections, J. Constr. Steel Res. 170 (2020) 106117.

[33] Saneinejad, A., Hobbs, B., Inelastic design of infilled frames, J. Struct. Eng. 121(4) (1995) 634-650.

[34] Qian, K., Lan, D.-Q., Fu, F., Li, B., Effects of infilled wall opening on load resisting capacity of RC frames to mitigate progressive collapse risk, Eng. Struct. 223 (2020) 111196.

[35] Qian, K., Lan, X., Deng, X.F., Li, Z., Effects of infilled walls with and without openings on progressive collapse resistance of steel frames under corner column loss condition, J. Struct. Eng. 149(8) (2023) 04023098.

[36] Kim, J., Lee, H., Progressive collapse-resisting capacity of framed structures with infill steel panels, J. Constr. Steel Res. 89 (2013) 145-152.

[37] Shan, S., Li, S., Wang, S., Effect of infill walls on mechanisms of steel frames against progressive collapse, J. Constr. Steel Res. 162 (2019) 105720.

[38] Qian, K., Lan, X., Li, Z., Fu, F., Behavior of steel moment frames using top-and-seat angle connections under various column-removal scenarios, J. Struct. Eng. 147(10) (2021) 04021144.

[39] Pirmoz, A., Khoei, A.S., Mohammadrezapour, E., Daryan, A.S., Moment-rotation behavior of bolted top-seat angle connections, J. Constr. Steel Res. 65(4) (2009) 973-984.

[40] Li, S., Kose, M.M., Shan, S., Sezen, H., Modeling methods for collapse analysis of reinforced concrete frames with infill walls, J. Struct. Eng. 145(4) (2019) 04019011.

[41] Qian, K., Lan, D.-Q., Li, S.-K., Fu, F., Effects of infill walls on load resistance of multi-story RC frames to mitigate progressive collapse, Structures 33 (2021) 2534-2545.

[42] Di Trapani, F., Giordano, L., Mancini, G., Progressive collapse response of reinforced concrete frame structures with masonry infills, J Eng Mech 146(3) (2020).

558 **List of figures**